








# Cerebral microvascular changes in healthy carriers of the APOE- $\epsilon$ 4 Alzheimer's disease risk gene

Rasmus Aamand <sup>a</sup>, Peter M. Rasmussen <sup>a</sup>, Katrine Schilling Andersen <sup>a</sup>, Stine de Paoli<sup>a</sup>, Eddie Weitzberg <sup>b,c</sup>, Michael Christiansen <sup>d,e</sup>, Torben E. Lund <sup>a</sup> and Leif Østergaard <sup>a,f,\*</sup>

<sup>a</sup>Department of Clinical Medicine, Center of Functionally Integrative Neuroscience (CFIN), Aarhus University, 8000 Aarhus, Denmark

<sup>b</sup>Department of Physiology and Pharmacology, Karolinska Institutet, 17177 Stockholm, Sweden

<sup>c</sup>Department of Perioperative Medicine and Intensive Care, Karolinska University Hospital, 17177 Stockholm, Sweden

<sup>d</sup>Department for Congenital Disorders, Statens Serum Institut, 2300 Copenhagen, Denmark

<sup>e</sup>Department of Biomedical Sciences, University of Copenhagen, 2200 Copenhagen, Denmark

<sup>f</sup>Department of Neuroradiology, Aarhus University Hospital, 8200 Aarhus, Denmark

\*To whom correspondence should be addressed: Email: [leif@cfin.au.dk](mailto:leif@cfin.au.dk)

Edited By Eric Klann

## Abstract

APOE- $\epsilon$ 4 is a genetic risk factor for Alzheimer's disease (AD). AD is associated with reduced cerebral blood flow (CBF) and with microvascular changes that limit the transport of oxygen from blood into brain tissue: reduced microvascular cerebral blood volume and high relative transit time heterogeneity (RTH). Healthy APOE- $\epsilon$ 4 carriers reveal brain regions with elevated CBF compared with carriers of the common  $\epsilon$ 3 allele. Such asymptomatic hyperemia may reflect *microvascular dysfunction*: a vascular disease entity characterized by suboptimal tissue oxygen uptake, rather than limited blood flow per se. Here, we used perfusion MRI to show that elevated regional CBF is accompanied by reduced capillary blood volume in healthy APOE- $\epsilon$ 4 carriers (carriers) aged 30–70 years compared with similarly aged APOE- $\epsilon$ 3 carriers (noncarriers). Younger carriers have elevated hippocampal RTH and more extreme RTH values throughout both white matter (WM) and cortical gray matter (GM) compared with noncarriers. Older carriers have reduced WM CBF and more extreme GM RTH values than noncarriers. Across all groups, lower WM and hippocampal RTH correlate with higher educational attainment, which is associated with lower AD risk. Three days of dietary nitrate supplementation increased carriers' WM CBF but caused older carriers to score worse on two of six aggregate neuropsychological scores. The intervention improved late recall in younger carriers and in noncarriers. The APOE- $\epsilon$ 4 gene is associated with microvascular changes that may impair tissue oxygen extraction. We speculate that vascular risk factor control is particularly important for APOE- $\epsilon$ 4 carriers' healthy aging.

**Keywords:** APOE- $\epsilon$ 4, Alzheimer's disease, cerebral blood flow, nitrate, relative transit time heterogeneity

## Significance Statement

Alzheimer's disease (AD) is associated with cerebral microvascular flow disturbances, which may be related to the vasoconstricting effects of amyloid protein build-up in the disease. Here, we report brain-wide microvascular flow disturbances in healthy carriers of APOE- $\epsilon$ 4, the main AD risk gene, before the typical age of amyloid protein build-up, and demonstrate that administration of a natural vasodilator modifies these disturbances and aspects of healthy subjects' brain functions. The identification of early brain changes in healthy subjects, who are at increased risk of developing AD in later life, allows us to develop targeted interventions that delay or prevent such changes. Such interventions are important in the efforts to reduce the burden of cognitive decline and dementia in our aging populations.

## Introduction

The  $\epsilon$ 4 allele of the APOE gene is associated with several-fold elevated risk of Alzheimer's disease (AD), so while only about 15% of the general population carry one or two versions of the  $\epsilon$ 4 allele, it is found in roughly 50% of patients with AD (1, 2). Patients with AD typically reveal reduced resting cerebral blood flow (CBF) (3) and impaired CBF responses to neuronal activation (4), but

asymptomatic APOE- $\epsilon$ 4 carriers reveal regions of elevated CBF during rest (2, 5–9) and higher task-related CBF responses than people with two versions of the common  $\epsilon$ 3 allele (10–12), independent of task performance (5, 13, 14), and dementia risk (15, 16).

Keeping in mind that brain tissue's oxygen uptake is the product of CBF and the oxygen extraction fraction (OEF), healthy APOE- $\epsilon$ 4 carriers' elevated CBF could, in principle, compensate

OXFORD  
UNIVERSITY PRESS

**Competing Interest:** L.Ø. is a minority shareholder and Scientific Advisory Board member in Cercare Medical AS, Denmark. E.W. is a named inventor on patents and patent applications relating to the medical uses of inorganic nitrate and nitrite and co-director of HeartBeet. The other authors declare no competing interests.

**Received:** May 8, 2024. **Accepted:** August 13, 2024

© The Author(s) 2024. Published by Oxford University Press on behalf of National Academy of Sciences. This is an Open Access article distributed under the terms of the Creative Commons Attribution-NonCommercial License (<https://creativecommons.org/licenses/by-nc/4.0/>), which permits non-commercial re-use, distribution, and reproduction in any medium, provided the original work is properly cited. For commercial re-use, please contact [reprints@oup.com](mailto:reprints@oup.com) for reprints and translation rights for reprints. All other permissions can be obtained through our RightsLink service via the Permissions link on the article page on our site—for further information please contact [journals.permissions@oup.com](mailto:journals.permissions@oup.com).

for age- and risk factor-related changes that limit oxygen extraction (17–19).

Biophysically, the extraction of oxygen from a single capillary is limited by blood's *capillary transit time*: the time available for blood–tissue oxygen diffusion exchange before blood returns to the heart (20) (see Fig. 1A). At the macroscopic level, blood's mean capillary transit time (MTT) can be calculated as the ratio between local capillary blood volume (CBV, milliliter blood per

milliliter tissue) and CBF (milliliter blood per milliliter tissue per minute), respectively (21). In normal brain tissue, CBV and CBF are both proportional to local metabolic demands during rest (22) and thus provide uniform MTT values across the brain, facilitating the extraction of oxygen from blood. During brain activation, however, CBF increases *without* proportional increases in CBV (23).

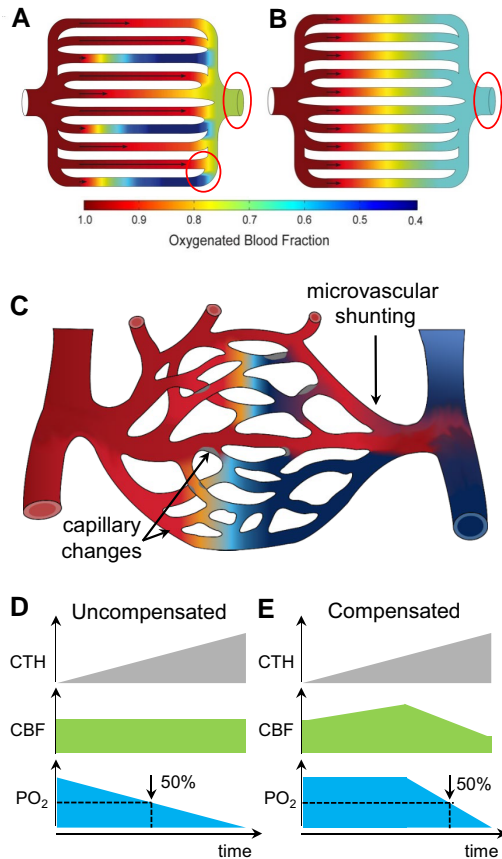
Figure 1A and B illustrates how capillary blood flows *homogenize* as CBF increases during brain activation (24–26) and thereby facilitate oxygen uptake. The accompanying *reduction* of capillary transit time *heterogeneity* (CTH) can indeed account for the brain's efficient oxygen extraction when metabolic demands and CBF increase, although CBV shows little change (27, 28). In fact, CTH—quantified as the SD of individual capillary transit times—decreases in proportion to their mean (MTT) in passive, compliant microvascular networks (27), providing a passive mechanism by which OEF remains high although MTT decreases during functional activation. The CTH/MTT ratio is termed the relative transit time heterogeneity (RTH) below.

Figure 1C illustrates how irreversible age- or risk factor-related *capillary changes*, which affect the resistance to blood flow through individual capillary segments, are expected to disturb the (re)distribution of capillary blood flows during rest (cf. Fig. 1A) and the homogenization of capillary transit times as CBF increases during brain activation (Fig. 1B). Note that while such changes limit blood flow through some capillary paths, they shorten blood's transit times through others, impairing oxygen extraction (20, 28, 29).

Figure 1D illustrates how a gradual increase in CTH, caused by the accumulation of such capillary changes over time, is predicted to reduce tissue oxygen levels if oxygen utilization and CBF remain constant. Figure 1E illustrates how *increasing* CBF is predicted to mitigate such tissue oxygen level reductions—until CTH reaches thresholds, where the benefit of higher blood supply, as a means to meet metabolic demands during rest and functional activation at physiological tissue oxygen levels, is outcompeted by its transit time-shortening effects (19, 20, 28, 29). Instead, subnormal CBF values yield longer MTT and permit more efficient oxygen extraction (higher OEF)—albeit at the expense of dwindling tissue oxygen levels (19). In other words, biophysical models predict that elevated resting CBF may compensate for (i.e. render asymptomatic) mild microvascular changes, whereas attenuation of CBF, paradoxically, is necessary to meet metabolic demands for more severe microvascular changes.

It is unknown whether the APOE-ε4 gene is associated with microvascular changes in the form of either reduced CBV or elevated RTH, and if so, whether this phenomenon is accompanied by altered CBF.

Dynamic susceptibility contrast (DSC) MRI (30) sensitized to capillary-sized vessels (31, 32) allows estimation of microvascular hemodynamics in humans (30). Cross-sectional (33–36) and longitudinal (37, 38) studies of healthy subjects at high risk of AD, subjects with mild cognitive impairment, and patients with AD, respectively, link the disease to loss of cortical microvessels (reduced CBV), decreasing CBF, and increasing CTH over time, particularly in cortical regions with amyloid-β (Aβ) aggregation (34–36), a pathological hallmark of AD that *antedates* memory symptoms by a decade or more (39). Aβ oligomers constrict human capillaries in AD by interfering with contractile capillary pericytes (40) and may thereby contribute to microvascular flow disturbances prior to any memory symptoms. Conversely, microvascular flow disturbances are believed to reduce the normal clearance of Aβ protein from brain tissue (41) and stimulate Aβ aggregation (42). To address APOE-ε4-related microvascular changes, subjects



**Fig. 1.** Blood's capillary transits and tissue oxygen extraction. Panels A–C illustrate blood's transition from being fully oxygenated arterial blood on the left to being partly deoxygenated venous blood on the right, passing through the tissue. A) Capillaries with high blood velocity (long arrows) provide short capillary transit times and therefore limited oxygen extraction, whereas capillaries with low flows (short arrows) provide efficient oxygen extraction (lower red circle). B) For the same blood flow and tissue oxygen tension as in panel A, a homogenous distribution of capillary blood flows provides a higher overall OEF—compare venular blood oxygenations (red ovals in panels A and B). Passive homogenization of capillary transit times as CBF increases explains tissue's efficient oxygen extraction during episodes of increased tissue metabolism. Adapted from (28). C) Age-, risk factor-, and disease-related capillary changes may affect oxygen extraction by preventing the redistribution of blood flow along individual capillaries according to cellular metabolic demands (cf. panel A) and the homogenization of capillary blood flows during episodes of increased metabolic demands (cf. panel B). D) Using CTH, the standard deviation of capillary transit times, as an index of the heterogeneity of capillary flows, the panel shows how accumulation of capillary changes (increasing CTH) over time causes tissue oxygen tension ( $PO_2$ ) to decline for a fixed metabolic rate and blood supply. E) For small increases in CTH, increased CBF is predicted to compensate for the reduction in OEF while maintaining physiological  $PO_2$ . Higher CBF shortens capillary transit times, however. Biophysically, attenuation of CBF is therefore predicted to sustain net oxygen extraction for more severe CTH increases. Note how these compensatory CBF changes delay the point at which hypoxia ensues (illustrated here as a 50% reduction in  $PO_2$ ). Modified from Østergaard (20).

should therefore be examined prior to when A $\beta$  aggregates begin to form in their brain tissue; thus, 15% of asymptomatic APOE- $\epsilon$ 4 homozygotes are estimated to be A $\beta$ -positive at age 40 years, while the corresponding age is 55 years for heterozygotes with the common APOE- $\epsilon$ 3 allele (43, 44).

This study compared microvascular hemodynamics in healthy APOE- $\epsilon$ 4 and APOE- $\epsilon$ 3 carriers aged 30–70 years for signs of reduced CBV, elevated RTH, and accompanying CBF changes. To address whether microvascular changes are reversible and affect brain functioning, we quantified these parameters before and after 3 days of vasodilator administration: dietary nitrate equivalent to a large, daily salad serving.

## Results

Subjects with at least one APOE- $\epsilon$ 4 allele ( $n = 38$ ; 29  $\epsilon$ 4/ $\epsilon$ 3 heterozygotes and 9  $\epsilon$ 4/ $\epsilon$ 4 homozygotes) are referred to as “carriers” below and APOE- $\epsilon$ 3 homozygotes ( $n = 38$ ) as “noncarriers.” See Fig. S1 for study groups and Table S1 for participant demographics.

Participants' CBF, CBV, and RTH were determined by spin echo DSC MRI. To the extent permitted by the spin echo MRI sequence's brain coverage, these parameters were first determined for three predefined regions of interest (ROIs): gray matter (GM), white matter (WM), and hippocampus (Fig. S2 B–D), and for cortical anatomical subregions for comparison with reports of elevated resting CBF in healthy APOE- $\epsilon$ 4 carriers by others. In the analyses of GM, WM, and hippocampus, subjects were dichotomized according to mean age so that “younger” and “older” refer to subjects aged  $\leq 52$  and  $> 52$  years, respectively. In the analyses of cortical subregions, age was used as a continuous variable for comparison.

### APOE- $\epsilon$ 4 is associated with elevated CBF but reduced CBV across cortical subregions

Carriers' average resting CBF values were higher in 11 cortical subregions compared with noncarriers ( $P < 0.01$ ), all of which overlapped with anatomical regions where this phenomenon was reported in the past (2, 5–7, 9) (see Fig. S3). Carriers' CBV was lower than in noncarriers in 11 cortical subregions ( $P < 0.01$ ; Fig. S4). Five of these subregions were among those displaying elevated CBF (Fig. S3). The APOE- $\epsilon$ 4 gene is thus associated with microvascular changes in the form of reduced CBV and accompanied by either preserved or elevated CBF.

Partial volume effects may interfere with CBF and microvascular density measurements, typically by underestimating values obtained in regions where the cortex is thin. Participants' cortical thickness correlated negatively with age ( $P < 0.01$ ) across subregions, but APOE genotype did not affect cortical thickness, nor interfere with this correlation (Fig. S5).

### APOE- $\epsilon$ 4 is associated with widespread microvascular changes in all carriers and low WM CBF in older carriers

In the subregion analysis, CBV was reduced in the hippocampus of APOE- $\epsilon$ 4 carriers compared with noncarriers (Fig. S4), while their average RTH was elevated (Table 1 and Fig. S7). This phenomenon was not accompanied by changes in hippocampal CBF (Fig. S3). See Figs. S6 and S7 for all age- and gene-specific ROI comparisons of RTH.

For WM and GM ROIs, average RTH values were identical across age and carrier groups, but compared with noncarriers, the spatial variability of RTH values was elevated across all tissue types in young carriers and in the GM of older carriers, implying that the

corresponding ROIs contain voxels with more extreme RTH values (see Table 2). In the subregion analysis (above), we noted a tendency for some anatomical GM regions to yield higher RTH values in carriers than in noncarriers ( $0.01 < P < 0.05$ ; Fig. S7) and no overlap with regions showing elevated CBF (Fig. S3). The WM ROI showed lower CBF in older carriers ( $n = 23$ ) compared with older noncarriers ( $n = 20$ ) (Table 1) but no significant differences in average RTH (Table 1) or RTH spatial variability (see Table 2).

We characterized the increased spatial variability of RTH values further by means of probability density functions that describe the distribution of RTH values within subjects' WM (Fig. 2A) and GM (Fig. 2B) ROIs, respectively, in the two APOE and age groups. Note that young noncarriers display the narrowest distribution of RTH values in both WM and GM. Figure 2C and D shows the gene-related difference between these distributions for younger and older subjects, respectively. Note how these differences mostly relate to carriers having more tissue with higher RTH values. The black lines highlight RTH ranges in which these differences are significant as determined by curve  $\chi^2$  differences. Figure 2E illustrates the location of voxels with RTH values within two such ranges (interval 3:  $1.05 < RTH < 1.23$  and interval 4:  $1.31 < RTH < 1.41$ ) for WM and GM cross younger noncarriers (left) and carriers (right). Thus, warmer colors indicate more subjects having RTH values within this range at the corresponding brain location. Keeping in mind that, biophysically, higher RTH is associated with poorer oxygen extraction, deep WM appears most severely affected by microvascular flow disturbances in younger APOE- $\epsilon$ 4 carriers. See Fig. S8 for the spatial distribution of values in other RTH ranges that displayed significant carrier–noncarrier differences.

White matter hyperintensities (WMHs) are radiological hallmarks of cerebral small vessel disease (cSVD) (45), and such lesions are known to affect RTH and CBF relative to surrounding normal-appearing WM in older subjects (46). Studies show WMHs to be more frequent in APOE- $\epsilon$ 4 carriers than noncarriers (47, 48), and we therefore examined the subjects with T<sub>2</sub>-weighted images ( $n = 59$ ) to determine WMH number and Fazekas scores (49). This analysis revealed similar WMH numbers and cSVD severity in carriers and noncarriers and low WMH load in younger subjects (see Fig. S9A and B). Group differences in RTH and CBF could therefore not be attributed to differences in WMH load.

### High educational attainment is associated with low RTH

Across age and carrier groups, more years of schooling was associated with lower RTH in the hippocampus, WM, and several cortical gray matter regions (see Figs. S6 and S7). This finding is notable in that more years of schooling is independently associated with lower AD risk (50, 51).

Partial volume effects may interfere with regional hemodynamic parameter estimates, and education attainment-related differences in tissue volumes could therefore bias RTH estimates toward these findings. However, we found no relation between educational attainment and regional cortical thickness (Fig. S5).

### Carriers and noncarriers show opposite CBF responses to nitrate supplementation

Nitric oxide (NO) is a mediator of vasodilation in brain arterioles and capillaries (52), and NO depletion within the vascular wall contributes to neurovascular dysfunction: the attenuated vasodilator responses observed in aging, hypertension, amyloidosis,





and APOE- $\epsilon$ 4 genotype (53–56). Oxygen availability limits NO synthesis from L-arginine via endothelial NO synthase, and hence, the vasodilation needed to restore oxygen levels, under hypoxic conditions (52). Mammals, however, can also produce NO from dietary nitrate via reactions that are particularly efficient at low oxygen levels (57, 58). Nitrate supplementation has proven safe in humans (59).

To examine whether modulation of perivascular NO levels affects CBF, CBV, and RTH across age and carrier groups, we subjected participants to 3 days of nitrate supplementation, equivalent to one daily, large salad serving, a dose previously shown to improve mitochondrial function in human muscle (60). Accordingly, subjects were given 0.1 mmol NaNO<sub>3</sub> sodium nitrate per kilogram bodyweight per day for 3 days in a randomized, double-blinded, placebo-controlled (NaCl ingestion) cross-over design (see Fig. S2A).

The intervention increased plasma nitrite and nitrate levels while lowering systolic blood pressure as expected (Tables S2 and S3) (61) and caused WM CBF to increase in carriers, whereas WM CBF tended to decrease in noncarriers (see Table 1 and Fig. S10). Whole-brain statistical analysis showed significant increases in carrier CBF across occipital, temporal, and frontal cortices (Fig. S2E).

### Nitrate supplementation modifies blood's microvascular distribution

Regional CBV values increased in response to nitrate supplementation (Fig. S13), whereas mean RTH remained unaffected (Fig. S12).

Figure S8 shows the WM and GM distributions of RTH values before (panels A and C) and after (panels E and G) nitrate ingestion across age and APOE groups. Note how these distributions are more similar after the intervention for GM (panel G), while the WM RTH distribution in young carriers seems to include more extreme RTH values after nitrate supplementation (panels E and F). Comparing the  $\chi^2$  differences between the nitrate and control session (Fig. S11), we notice that nitrate ingestion mostly affects the distributions of RTH values in carriers.

### Nitrate supplementation and neurocognitive functions: paradox responses in older carriers

All subjects underwent a battery of six neuropsychological tests after the nitrate and placebo (NaCl) conditions, respectively, immediately before and after their MRI examinations. The resulting 24 scores were subjected to principal component analysis (PCA) to reduce score interdependency across test batteries, resulting in six largely distinct clusters (see Tables S4 and S5). The neuropsychological tests did not reveal major changes in subjects' performance after nitrate supplementation, with notable exceptions: Nitrate supplementation improved the ability to recall and redraw complex figures after 3 and 30 min in the Rey–Osterrieth complex figure (ROCF) test (Table S4, cluster 6) (62) in all participants except the older carriers, who performed worse (Table S5). Also, nitrate supplementation significantly prolonged the time taken by older carriers to complete the trail making tests A and B (63) compared with the placebo condition (Table S5).

## Discussion

The first main finding of this study is that APOE- $\epsilon$ 4 carriers reveal microvascular changes that are thought to limit the transport of oxygen from blood into brain tissue: reduced CBV and high RTH.

Thus, carriers had cortical subregions with reduced CBV (Fig. S13) and elevated RTH in gray matter as a whole (Table 2). Consistent with earlier reports (2, 5–9), carriers revealed 12 cortical regions with elevated resting CBF, five of which corresponded to regions with low CBV, consistent with the notion that CBF may be increased to compensate for the resulting shortening of capillary transit times. Our findings are consistent with earlier findings of reduced microvascular density in the neocortex, corpus callosum (55) and hippocampus (64, 65) of mice carrying the human APOE- $\epsilon$ 4 gene.

Younger carriers, who are not yet suspected of amyloid pathology (43, 44), reveal microvascular flow disturbances in the form of elevated RTH values in their hippocampi (Table 1) and widespread, abnormally high RTH values in image voxels across their GM (Table 2 and Fig. 2D) and WM (Table 2 and Fig. 2C). These observations suggest that the microvascular changes are characteristic of the APOE- $\epsilon$ 4 gene, rather than results of early build-up of A $\beta$  protein, which acts as a capillary constrictor (40). While amyloid pathology generally spares the hippocampus in AD, the hippocampal microcirculation is thought to be particularly vulnerable (66).

The second main finding is that WM CBF is reduced in healthy, older APOE- $\epsilon$ 4 carriers. The dysregulation of microvascular transit times observed in younger carriers' WM (Table 2 and Fig. 1C and E) could herald severe microvascular flow disturbances in later life, suggesting that older carriers' lower WM CBF, paradoxically, may counteract the biophysical effects of such changes (Fig. 1). The defining feature of compensatory reductions of CBF to counteract poor oxygen extraction, as opposed to a primary reduction in CBF due to neurovascular dysfunction, is that "normalization" of CBF is expected to reduce tissue oxygenation in the former. Older carriers' resting WM CBF was indeed lower than that of noncarriers, but their neuropsychological scores deteriorated although their WM CBF increased after nitrate supplementation. This is consistent with a paradox reduction of oxygen extraction that negatively affects neuronal network activity—contrary to the current understanding of the relation between blood flow and tissue oxygenation and warrants further study. Nonetheless, if microvascular dysfunction is accompanied by tissue oxygen depletion, it could contribute to the WM vulnerability associated with the APOE- $\epsilon$ 4 allele (55), including the propensity of carriers to develop WMHs (47, 48).

Previous studies show evidence of progressive and severe, cortical microvascular flow disturbances in patients with AD (33, 38), and recent studies of patients with mild cognitive impairment suggest a transition from mild to severe microvascular flow disturbances around the time that subjective memory symptoms appear, linked in part to the vasoconstrictor properties of amyloid protein (34, 35, 37). The current study suggests that APOE carrier status and WM microvascular function may be important to our understanding of the earliest stages of AD, and to future, targeted prevention strategies.

In terms of risk factors, the study unexpectedly found that RTH in the hippocampus, WM, and several cortical gray matter regions was inversely correlated with participant education years, irrespective of carrier and age group, possibly offering a physiological contributor to the puzzling relation between high educational attainment and low AD risk. Learning introduces profound, adaptive changes in both WM and GM cytoarchitecture (67, 68), paralleled by dynamic adaptations of the microcirculation to meet the associated energy costs, particularly of maintaining synapses (69). Such adaptations not only include angiogenesis and higher capillary density in cortical layers with high synaptic

Table 2. LME analysis of the regional variability of perfusion values.

y	Fixed effect	White matter						Grey matter						Hippocampus						
		Full model			Reduced model			Full model			Reduced model			Full model			Reduced model			
		P	Est.	SE	P	Est.	SE	P	Est.	SE	P	Est.	SE	P	Est.	SE	P	Est.	SE	
CBF	Intercept	0.000	0.06	0.01	0.00	0.06	0.00	0.000	0.22	0.02	0.02	0.00	0.00	0.10	0.01	0.000	0.256	0.10	0.01	Full model not sign. better than null model
	Age	0.873	0.00	0.01				0.625	-0.01	0.03	0.03			-0.01	0.01	0.256	0.00	0.01	0.01	
	APOE	0.749	0.00	0.01				0.803	-0.01	0.03	0.03			0.00	0.01	0.973	0.00	0.01	0.01	
	Gender	0.717	0.00	0.01				0.368	-0.02	0.02	0.02			-0.01	0.01	0.547	-0.01	0.01	0.01	
	Nitrate	0.234	-0.01	0.00	0.018	-0.01	0.00	0.076	-0.03	0.02	0.02			-0.01	0.01	0.400	0.00	0.01	0.01	
	Session	0.186	0.01	0.00	0.002	0.01	0.00	0.318	0.02	0.02	0.02			0.00	0.01	0.765	0.00	0.01	0.01	
	Educational years	0.829	0.00	0.00				0.112	0.00	0.00	0.00			0.00	0.00	0.153	0.00	0.00	0.00	
	Height	0.000	0.00	0.00	0.000	0.00	0.00	0.056	0.00	0.00	0.00	0.002	0.00	0.00	0.00	0.159	0.00	0.00	0.00	
	Weight	0.173	0.00	0.00				0.675	0.00	0.00	0.00			0.00	0.00	0.435	0.00	0.00	0.00	
	Age x APOE	0.188	-0.02	0.01	0.002	-0.02	0.01	0.282	-0.04	0.04	0.04	0.002	-0.06	0.02	0.02	0.947	0.00	0.02	0.02	
	Age x Nitrate	0.795	0.00	0.01				0.367	0.02	0.02	0.02			0.01	0.01	0.428	0.01	0.01	0.01	
	APOE x Nitrate	0.005	0.02	0.01	0.000	0.02	0.00	0.005	0.07	0.03	0.03	0.017	0.03	0.01	0.01	0.100	0.02	0.01	0.01	
	Age x Session	0.352	-0.01	0.01	0.028	-0.01	0.00	0.079	-0.04	0.02	0.02	0.002	-0.03	0.01	0.01	0.429	-0.01	0.01	0.01	
	APOE x Session	0.141	0.01	0.01				0.332	0.03	0.03	0.03	0.002	0.04	0.01	0.01	0.807	0.00	0.01	0.01	
	Age x APOE x Nitrate	0.354	-0.01	0.01				0.159	-0.05	0.04	0.04			-0.01	0.01	0.278	-0.01	0.01	0.01	
Age x APOE x Session	0.376	-0.01	0.01				0.710	0.01	0.04	0.04			0.01	0.01	0.432	0.01	0.01	0.01		
CBV	Intercept	0.000	23.96	1.50			0.000	33.38	1.84	1.84			0.000	30.65	1.88	0.000	0.000	1.88	1.88	
	Age	0.207	-2.65	2.09			0.300	-2.64	2.54	2.54			0.513	1.70	2.60	0.513	1.70	2.60	2.60	
	APOE	0.975	-0.07	2.15			0.550	-1.55	2.59	2.59			0.876	0.41	2.64	0.876	0.41	2.64	2.64	
	Gender	0.357	-1.44	1.55			0.934	-0.16	1.97	1.97			0.402	1.71	2.04	0.402	1.71	2.04	2.04	
	Nitrate	0.977	0.03	1.15			0.595	0.67	1.26	1.26			0.574	0.69	1.23	0.574	0.69	1.23	1.23	
	Session	0.158	-1.63	1.15			0.017	-3.06	1.26	1.26			0.247	-1.42	1.23	0.247	-1.42	1.23	1.23	
	Educational years	0.381	0.15	0.17			0.570	0.12	0.21	0.21			0.432	0.17	0.22	0.432	0.17	0.22	0.22	
	Height	0.008	-0.27	0.10	0.000	-0.309	0.077	0.005	-0.36	0.13	0.13	0.000	-0.351	0.095	0.086	-0.23	0.086	0.13	0.13	
	Weight	0.000	0.24	0.05	0.000	0.234	0.045	0.000	0.33	0.06	0.06	0.000	0.320	0.056	0.000	0.35	0.06	0.06	0.06	
	Age x APOE	0.575	1.64	2.92			0.346	3.34	3.53	3.53			0.993	-0.03	3.60	0.993	-0.03	3.60	3.60	
	Age x Nitrate	0.707	0.63	1.66			0.825	-0.41	1.83	1.83			0.175	-2.42	1.78	0.175	-2.42	1.78	1.78	
	APOE x Nitrate	0.706	0.67	1.77			0.702	0.75	1.95	1.95			0.621	0.94	1.89	0.621	0.94	1.89	1.89	
	Age x Session	0.079	2.95	1.66			0.051	3.61	1.83	1.83			0.986	0.03	1.78	0.986	0.03	1.78	1.78	
	APOE x Session	0.105	2.89	1.77			0.007	5.36	1.95	1.95	0.037	1.919	0.909	0.88	1.89	0.643	0.88	1.89	1.89	
	Age x APOE x Nitrate	0.540	-1.47	2.39			0.474	-1.89	2.63	2.63			0.775	0.73	2.55	0.775	0.73	2.55	2.55	
Age x APOE x Session	0.213	-2.99	2.39			0.109	-4.25	2.63	2.63			0.395	2.18	2.55	0.395	2.18	2.55	2.55		
RTH	Intercept	0.000	0.12	0.01	0.00	0.12	0.00	0.000	0.15	0.01	0.01	0.00	0.12	0.01	0.000	0.000	0.12	0.01	0.01	
	Age	0.675	0.01	0.01			0.369	0.01	0.01	0.01			0.093	0.03	0.02	0.093	0.03	0.02	0.02	
	APOE	0.007	0.04	0.01	0.000	0.04	0.01	0.006	0.04	0.02	0.02	0.005	0.02	0.01	0.006	0.05	0.02	0.02	0.02	
	Gender	0.110	-0.01	0.01	0.022	-0.01	0.01	0.493	-0.01	0.01	0.01			0.00	0.01	0.711	0.00	0.01	0.01	
	Nitrate	0.476	0.01	0.01			0.334	0.01	0.01	0.01			0.510	0.01	0.01	0.510	0.01	0.01	0.01	
	Session	0.687	0.00	0.01			0.654	0.00	0.01	0.01			0.818	0.00	0.01	0.818	0.00	0.01	0.01	
	Educational years	0.068	0.00	0.00	0.043	0.00	0.00	0.080	0.00	0.00	0.00			0.00	0.01	0.077	0.00	0.01	0.01	
	Height	0.796	0.00	0.00			0.919	0.00	0.00	0.00			0.546	0.00	0.00	0.546	0.00	0.00	0.00	
	Weight	0.712	0.00	0.00			0.879	0.00	0.00	0.00			0.304	0.00	0.00	0.304	0.00	0.00	0.00	
	Age x APOE	0.078	-0.03	0.02	0.001	-0.04	0.01	0.155	-0.03	0.02	0.02			-0.06	0.02	0.012	-0.06	0.02	0.02	
	Age x Nitrate	0.663	-0.01	0.01			0.368	-0.01	0.02	0.02			0.262	-0.02	0.02	0.262	-0.02	0.02	0.02	
	APOE x Nitrate	0.862	0.00	0.02			0.618	-0.01	0.02	0.02			0.927	0.00	0.02	0.927	0.00	0.02	0.02	
	Age x Session	0.979	0.00	0.01			0.981	0.00	0.02	0.02			0.187	-0.02	0.02	0.187	-0.02	0.02	0.02	
	APOE x Session	0.054	-0.03	0.02	0.003	-0.036	0.012	0.060	-0.03	0.02	0.02	0.033	-0.018	0.008	0.016	-0.05	0.02	0.02	0.02	

(continued)

Table 2. Continued

y	Fixed effect	White matter						Grey matter						Hippocampus						
		Full model			Reduced model			Full model			Reduced model			Full model			Reduced model			
		P	Est.	SE	P	Est.	SE	P	Est.	SE	P	Est.	SE	P	Est.	SE	P	Est.	SE	
	Age × APOE × Nitrate	0.655	-0.01	0.02	0.011	0.039	0.015	0.696	-0.01	0.02	0.02	0.858	0.00	0.03	0.009	0.07	0.03	0.016	0.05	0.02
	Age × APOE × Session	0.081	0.04	0.02	0.011	0.039	0.015	0.187	0.03	0.02	0.009	0.07	0.03	0.016	0.05	0.02	0.03	0.016	0.05	0.02

Regional variability was quantified by the mean absolute deviation (MAD) as described in "Materials and methods." A × B in the table indicates an interaction, i.e. that the effects are not additive but depends on their state. Bold P values indicate a significant effect (AU). P values in italic indicate a tendency. SE refers to the standard error of the estimate. The estimate refers to the estimate of the fixed effect. This estimate should thus be added in the model for participants being: older, ε4, male, on nitrate, having more education years, etc., or the combined effect of these fixed effects. That is, in this table the LME estimates that 0.02 should be added to our WM CBF estimate if the participants have had nitrate and have an ε4 allele; otherwise not.

density (22), but also changes in capillary bed topology that permit more homogenous capillary blood flow and higher OEF in those cortical layers, relative to neighboring layers that share the same blood supply and tissue oxygen tension (70). We speculate that learning and memory-induced microvascular adaptations include such topological optimizations in relation to the cellular populations involved. Widespread and continuing microvascular adaptation to higher oxygen extraction yields (lower RTH), in turn, might offer resilience to the accumulation of age- and risk factor-related capillary damage (increasing RTH), which seemingly plays a role in the development of AD.

## Effects of nitrate supplementation on vascular function and cognitive performance

The effects of dietary nitrate supplementation on neuropsychological functioning and on cerebral hemodynamics and blood oxygenation have been examined in several studies, yielding inconclusive results (59). These studies included relatively few healthy participants (10–40) in different age groups (the mean age ranging from 20 to ≥ 70) and a wide range of nitrate doses (5–24.2 mmol/day) and intervention durations (90 min after a single dose—10 weeks). Our results suggest that age and APOE-ε4 genotype, combined, affect the direction of changes in regional CBF and neurocognitive function after nitrate supplementation.

It should be kept in mind that neurovascular dysfunction is characterized not only by reduced NO bioavailability, but also oxidative injury to the microcirculation. The potential benefits of dietary nitrate supplementation may therefore be greatest before neurovascular dysfunction becomes apparent, at which time microvascular changes may still be reversible. Dietary supplementation should therefore be tested in well-powered trials controlled for age, APOE-ε4 genotype, hypertension, and other risk factors that might interact with capillary function.

## Limitations to the study

This study measured parameters that, biophysically, limit the transport of oxygen from blood into brain tissue (reduced CBV and high RTH), rather than oxygen extraction per se. Direct measurements of OEF in cortical layers with high metabolic demands confirm that more homogenous (resting) capillary blood flows allow tissue to extract a higher proportion of bloods oxygen content without lowering tissue oxygen tension (70)—consistent with the biophysical importance of capillary transit times (20, 28). The dependence of OEF upon blood's microvascular distribution in human brain, as measured by gold-standard positron emission tomography OEF and the MRI method applied in this study, respectively, was confirmed in patients with large-vessel disease (71) but should be verified in larger studies.

The impact of bloods microvascular distribution on brain oxygenation was only recognized recently, and assessment of this hemodynamic property in humans is inherently difficult. Characterizing blood's capillary transit times based on the passage of exogenous contrast media (CM) passages through MRI voxels that contain up to 200,000 capillary segments totaling ~12 m in length (72) therefore rely on a number of assumptions that are discussed in (30). Notably, relative flow heterogeneity (analog to RTH) is believed to be fractal across the vascular tree, that is, apply to the distribution of blood flow from the level of capillary ensembles to entire organs (73), supporting the interpretation of voxel-wise, or even organ-wide, transit time distributions in terms micrometer-scale hemodynamics. Indeed, RTH estimates based on the indicator dilution method used in this study have yielded similar and

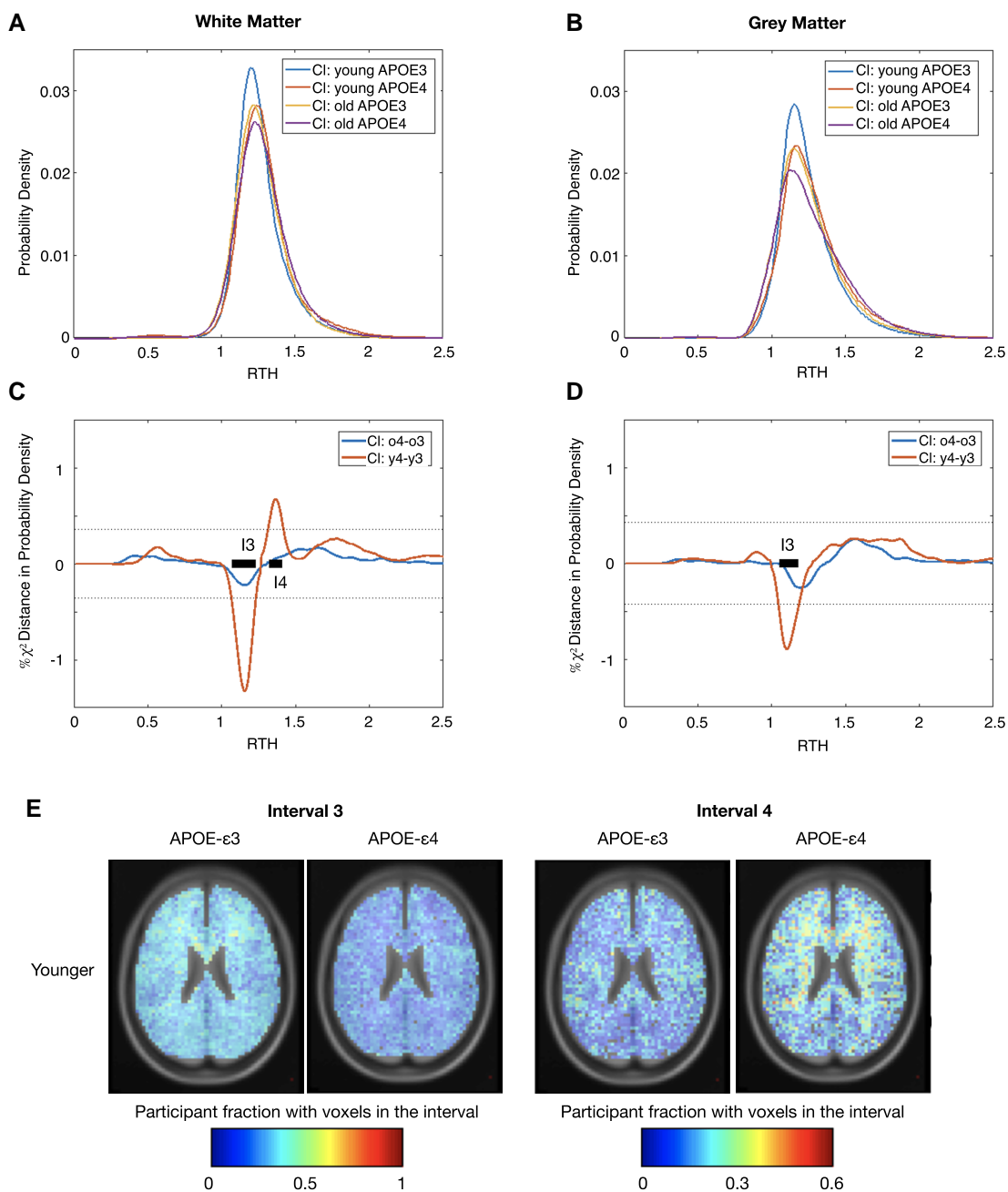


**Fig. 2.** Spatial view on RTH. To establish whether the variations in RTH across the GM and WM ROIs reflected a structured spatial pattern or simply differences in random locations, we calculated probability density functions (pdfs) of the RTH values in WM (A) and GM (B) during the control and nitrate session (see Fig. S8 for all differences according to carrier and age group, GM/WM, and session). We defined five separate intervals (I1–I5) representing the 5% largest  $\chi^2$  differences (those surpassing the dotted lines in C and D) between the younger and older and carriers and noncarriers in WM (C) and GM (D). Here, only differences in the control session between older and younger carriers and noncarriers (o4–o3 and y4–y3) are shown. Interval-specific RTH values were consequently localized in each participant and summed for each participant group. Thus, E shows the distribution of image voxels with values in the I3 (left) and I4 (right) intervals across the younger participants. Note how younger carriers had less voxels in the I3 interval and more in the I4 interval compared with the young noncarriers. y3: younger noncarriers; o3: older noncarriers; y4: younger carriers; o4: older carriers.

consistent results when applied to patients with AD and controls using DSC MRI (33) and to AD models and controls using two-photon laser microscopy at the level of individual microvessels (74).

Our study sample was relatively small, which may have affected our ability to detect microvascular flow disturbances in WM and hippocampi further. Future studies should also examine a sufficient number of APOE- $\epsilon 4/\epsilon 4$  homozygotes to examine whether the extent of capillary flow disturbances displays a gene dose–response similar to their AD risk.

Hippocampi were the brain structures most affected by microvascular flow disturbances in young carriers. Our DSC MRI methods are somewhat sensitive to brain motion and susceptibility artifacts in this brain region. Also, due to the oblong shape and limited volume of the hippocampi, image voxels in this region tend to contain contributions from surrounding tissue and fluids—so-called partial volume effects. Therefore, far fewer DSC voxels are classified as belonging to the hippocampi than are voxels within WM and GM, respectively. We speculate that this limited our



sensitivity to detect CBF and RTH changes in these critical brain structures.

## Materials and methods

### Ethical approval and informed consent

The study was approved by the Ethics Committee of the Central Denmark Region (Project-ID: M-2013-239-13) and conducted in accordance with the Helsinki Declaration. All participants gave written informed consent prior to their participation.

### Participant recruitment

Initially, 283 healthy participants between 30 and 70 years of age were recruited from the public through advertisements in a local newspaper. All participants were required to (i) have Danish as their main language, (ii) have no diagnosed neuropsychiatric disorders, nor use prescription drugs, (iii) have no prostheses, pace-makers, etc., that could interfere with the MR scans, (iv) not suffer from claustrophobia, (v) not be obese, (vi) not suffer from anxiety related to blood or needles, (vii) have normal kidney function, (viii) not be pregnant, (ix) not have a history of frequent or major allergic reactions, and (x) have no gross anatomical abnormalities on brain MRI.

All participants underwent genetic screening to establish their APOE allele status. Out of the 283 participants, we included 52 carriers of at least one APOE- $\epsilon$ 4 allele (14  $\epsilon$ 4/ $\epsilon$ 4 and 38  $\epsilon$ 3/ $\epsilon$ 4) and 48 carriers of two APOE- $\epsilon$ 3 alleles. The two groups were balanced in terms of gender and distribution of age across the four decades from 30 to 70 years of age. The mean age of 52 years instead of 50 years was caused by late participant cancellations and older participants more readily accepting to show up.

### Participant dropout

Five participants did not complete the study. Reasons included participants not showing up to be scanned and participants feeling uncomfortable. The dropouts are described in Fig. S1. Of the remaining 95 participants, four participants were excluded due to incorrect or missing nitrate intake as indicated by their blood nitrate/nitrite samples, and two participants were excluded because of lost samples/lost data. Hence, 89 participants were included in the analyses of cognitive tests, blood pressure, and blood samples. For the MR perfusion analyses, data from 76 participants were included in the analyses. Reasons for excluding patients from MR examinations included insufficient kidney function (estimated glomerular filtration rate [eGFR] < 60 ml/min/1.73 m<sup>2</sup>) as proper kidney function is a prerequisite for perfusion MRI using gadolinium (Gd)-based CM. Also, participants whose head size exceeded the dimensions of our MR systems head coil were excluded.

### Study drug and placebo

The study was a randomized, double-blinded, placebo-controlled cross-over study, during which participants ingested either sodium nitrate (0.1 mmol NaNO<sub>3</sub> per kg bodyweight per day, Sigma-Aldrich, MO, USA) or sodium chloride (0.1 mmol NaCl per kg bodyweight per day as a control) for 3 days. This nitrate dose mimics a large serving of nitrate-rich vegetables and resembles that of a study of beetroot juice, CBF, and cognitive performance in normal volunteers (75, 76).

Tests and imaging were carried out on the third day of ingestion, and the drug/placebo studies were separated by a washout period of a minimum of 10 days (Fig. S2A). The saline solutions

were mixed with concentrated fruit juice to disguise differences in taste. The saline solutions were prepared by R.A. and their content blinded by a researcher not otherwise involved in the experiment. Solutions were tested for nitrite every day, and no sign of conversion was seen.

### Food restrictions

A food regimen was implemented to prevent participants from ingesting vegetables with high levels of nitrate or nitrite (77) and food sources containing high levels of vitamin C, which may augment the conversion rate of nitrite into NO. Accordingly, during the 3-day periods of salt solution ingestion, participants were to abstain from eating green leafy vegetables, brassicas, beet root, pepper fruits, and radish. Participants were also asked to avoid eating strawberries, citrus fruits, rhubarb, nuts, and processed meats.

### Blood data

#### Genotyping

For the initial screening for APOE genotype, venous blood samples were collected into ethylenediaminetetraacetic acid (EDTA) tubes and stored on ice. Centrifugation (2,000g, 10 min, 4°C) and separation of plasma, buffy coat, and red blood cells were completed within an hour, and samples were stored at -80°C until genotyping. APOE genotype was determined at Statens Serum Institut, Copenhagen (MC).

#### Blood biomarkers

In the main experiment, one blood sample was collected prior to each 3-day salt ingestion period and an additional blood sample was acquired immediately before the MR scanning session was commenced on day 3. Blood samples were analyzed at Aarhus University Hospital's Department of Clinical Biochemistry. Total plasma cholesterol, plasma high-density lipoprotein (HDL) cholesterol, and plasma creatinine levels were measured on a Cobas 6000 C system. Plasma low-density lipoprotein (LDL) cholesterol was calculated as the difference between total plasma cholesterol and HDL cholesterol. The eGFR was calculated from plasma creatinine levels and corrected for age and gender.

#### Nitrate/nitrite

Before each saline ingestion period and immediately before and after each MR scanning session, blood samples for plasma nitrate and nitrite quantification were collected in low-nitrite EDTA tubes, manufactured for this purpose and provided by the Karolinska Institute, Stockholm, Sweden (EW). Samples were immediately centrifuged (5,000 g, 5 min, 4°C) and after separation into red blood cells, buffy coat, and plasma instantaneously placed on ice and moved to -80°C storage. All measurements of nitrite and nitrate content in the plasma fraction were taken at the Department of Physiology and Pharmacology, Section of Anesthesiology and Intensive Care, Karolinska Institute, Stockholm, Sweden (EW). The nitrate and nitrite levels during MR were calculated as the average before and after the MR scan.

### Physiological data

#### Blood pressure

Blood pressure was measured in the MR scanner using a Medrad Veris MR Vital Signs Monitor (Warrendale, USA). Measurements were taken before and after each perfusion scan. Participants were lying down quietly in the scanner for at least 45 min prior to blood pressure measurements and perfusion scans.

### Transcutaneous blood gas measurements

The oxygen saturation (SpO<sub>2</sub>) and carbon dioxide tension (PCO<sub>2</sub>) in the blood was measured noninvasively and continuously across the skin just below the eye of the participants. This was done using a transcutaneous Sentec V-Sign sensor (SENTEC-AG, Therwil, Switzerland) adapted for use in the MRI environment as described in Fig. S1 of Rasmussen (78). The data were recorded using a Brain Vision BrainAmp ExG MR Amplifier (Gilching, Germany) connected to a PC.

### Neuropsychological assessment

Sporadic AD is associated with deteriorating cognitive abilities, including executive functioning, visual spatial functioning, and episodic, working and spatial memory (79, 80). To probe these domains, participants underwent a battery of neuropsychological tests, including (i) Wechsler Adult Intelligence Scale-Fourth Edition digit span (forward/backward and sequencing), vocabulary (in Danish), and block design subtests (81), (ii) ROCF test (copy, recall after 3 and 30 min) (62), (iii) two text recall subtests from Wechsler Memory Scale-III (82), (iv) Ruff light trail learning test I and II (83), (v) Raven's progressive matrices (84), and (vi) trail making test A and B (63). The tests were carried out either before or after the MRI scans by staff supervised and trained by experienced neuropsychologists (SdP).

### Magnetic resonance imaging

All participants were imaged in a supine position using a Magnetom Skyra 3.0-T MRI system (Siemens, Erlangen, Germany).

#### Anatomical T1 MRI

Anatomical images were recorded using a magnetization-prepared two rapid acquisition gradient echoes (MP2RAGE) sequence with 1-mm<sup>3</sup> isotropic voxels using time of echo (TE) = 2.98 ms, time of repetition (TR) = 5,000 ms, inversion times 700 and 2,500 ms, acquisition matrix = 240 × 256 × 176, flip angle (FA) = 4° and 5°, echo spacing 7.1 ms, and iPAT factor 2 (GRAPPA).

#### Perfusion MRI

To measure cerebral perfusion, we performed DSC MRI, using a spin echo sequence, which, for short echo times and acquisition windows, is weighted toward microvessels in the 5–15- $\mu$ m range (31, 85).

Dynamic spin echo echo planar imaging (EPI) MR images were recorded during the bolus injection of 0.2 mmol/kg per kg body-weight Gadovist, a Gd-based CM (gadobutrol, Bayer, Denmark), followed by a 30-ml saline flush. All injections were carried out at a speed of 5 mL/s using a Medrad (Warrendale, PA, USA) Spectris Solaris EP MR injection system, controlled by an in-house trigger system, which allows us to link CM injection to a certain point in the dynamic image acquisition. The imaging sequence comprised 300 dynamic acquisitions, 200 of which were acquired prior to CM injection. The imaging parameters were: TE = 60 ms, TR = 1,530 ms, acquisition matrix = 64 × 64 × 19, FA = 90° and 180°, and voxel size 3 × 3 × 3 mm<sup>3</sup> with a 1-mm gap between slices. The spin echo EPI images were acquired with an iPAT factor of 3 and an echo spacing of 0.5 ms, resulting in a readout window of (64/3) × 0.5 ms = 10.7 ms.

#### FLAIR images

The FLAIR images used for quantifying the WMH originated from a diffusion kurtosis imaging (DKI) measurement taken during the second examination of each subject. To avoid cerebrospinal fluid

(CSF) contamination in the DKI measurements, we applied a 2,100-ms inversion pulse prior to radiofrequency (RF) excitation. Accordingly, the non-diffusion weighted images had contrast similar to a conventional FLAIR image. Using EPI images for FLAIR contrast has recently been found adequate (86). The sequence parameters were as follows: TE = 101 ms, TR = 24.8 s, acquisition matrix 96 × 96 × 76, FA = 180°, 90°, and 180°, and voxel size 2.3 × 2.3 × 2 mm<sup>3</sup> with no gap between slices. The images were acquired with both blip-up and blip-down phase encoding and were subsequently distortion corrected using TOPUP (87) from the FSL software (<https://fsl.fmrib.ox.ac.uk/fsl/fslwiki/topup>).

### Data analysis tools

All data were processed in MATLAB (MathWorks, Massachusetts, USA), release R2016b. For MR data analysis, we used SPM12 (release 6685, University College London, UK) and an in-house data processing pipeline for perfusion MRI analysis.

### Analysis of blood data and physiological data

#### Missing data—nitrate/nitrite

Missing preingestion values ( $n = 4$ ) were assigned the median value of all preingestion values. Missing pre-MRI values and missing post-MRI values ( $n = 3$ ) were assigned the median value of the subject's group (carrier/noncarrier), time (pre/post), and treatment (NaCl/NaNO<sub>3</sub>). We chose this approach because nitrate/nitrite levels were used as indicators of correct saline ingestion rather than as an outcome measure.

#### Missing data—blood pressure

Participants with missing data were excluded from the analyses. The minimal value of the three blood pressure measurements taken during each scan session was used in the statistical analyses.

#### Alignment—transcutaneous SpO<sub>2</sub> and PCO<sub>2</sub> and perfusion MRI

The recordings were used as continuous covariates in the voxel-wise SPM analysis of perfusion data to control for their influence on cerebral hemodynamics. To obtain a representative value for SpO<sub>2</sub> and PCO<sub>2</sub> during the CM bolus passage used to calculate perfusion indices, we used their mean value starting at the time of CM injection and throughout the subsequent 30 dynamic image volumes (~45 s).

### Analysis of neuropsychological tests

At every experimental session, each subject's cognitive performance was characterized by 24 test scores, each summarizing the subject's performance on subtests taken from the six neuropsychological tests. To disentangle the interdependency of test scores and to group test scores according to separate aspects of neurocognitive function, we applied PCA across the two sessions in all subjects. Using this data-driven approach, we identified the six subtest clusters given in Table S4. The observed clustering was expected based on the nature of the subtests and the neurocognitive domains they probe, except the ROCF copying task scores, which grouped with fluid intelligence scores rather than the remaining ROCF scores. To summarize cognitive performance within each cluster, we applied PCA within each cluster to the mean-centered test scores scaled by their standard deviation from all subjects. PCA thus provides the linear combination of subscores along which within-cluster subscore variance is maximized. For each cluster, we retained the first principal component to use in the statistical analyses. See Table S4 for the percentage

of within-cluster subscore variance accounted for by the six PCA-derived composite scores based on cluster subscores.

## Perfusion MRI analysis

### Preprocessing and concentration curves

Dynamic DSC image volumes were motion corrected to a reference volume defined by the participants' head location immediately before CM injection. The images volumes were slice-time corrected and co-registered to anatomical (T1-weighted) images. The relative CM concentration time curve,  $C(t)$ , was calculated in each voxel based on its average intensity during the baseline scans prior to bolus passage  $S_{t0}$  and the resulting signal time curve

$$C(t) = -\frac{1}{TE} \ln\left(\frac{S(t)}{S_{t0}}\right),$$

where TE is the EPI sequences TE and  $S(t)$  the  $T_2$ -weighted signal intensity in the voxel at time  $t$ .

### Arterial input function selection

Perfusion data analysis relies on the choice of an arterial input function (AIF) to represent the shape of the CM concentration time curve in the arterial supply of tissue within image voxels (88). Comparisons of perfusion values among subjects or across sessions in single subjects are therefore sensitive to the fidelity of the AIF, which in turn depends on the choice of arterial voxels (89, 90). AIF selection was thus performed as a two-step to ensure that AIFs were recorded at comparable locations in the two sessions. In the first step, an initial voxel selection was conducted. 500 voxels from each session with the fastest time to peak and the greatest area under the concentration time curve until peak was identified as potential AIF voxels. To do so, we used the algorithm previously described by Mouridsen et al. (91). In the second step, voxels identified as potential AIFs in both sessions were subjected to the same algorithm again, but only allowing six voxels to remain in each session. These six voxels were used to construct a mean AIF curve for each session and used to calculate perfusion maps. See Fig. S14 for a summary image of the AIF voxel positions.

### Calculating perfusion maps

According to indicator dilution theory, the concentration CM in any voxel,  $C(t)$ , can then be seen as a convolution of  $C_a(t)$

$$C(t) = \text{CBF} \int_0^t C_a(\tau) R(t - \tau) d\tau,$$

where  $R(t)$  denotes the residue function, that is, the fraction of CM still present in the voxel at time  $t$  after an infinitely narrow impulse injection into its feeding artery (88).  $R(t)$  can be estimated using a parametric approach based on an anatomical model of the microvasculature (92). The approach approximates the transport function  $h(t)$  for CM as it passes through the vasculature by a family of gamma distributions

$$h(t; \alpha, \beta) = \frac{1}{\beta^\alpha \Gamma(\alpha)} t^{\alpha-1} e^{-t/\beta}, \quad \alpha, \beta > 0,$$

where

$$R(t) = \int_t^\infty h(t; \alpha, \beta) dt,$$

and  $\alpha$  and  $\beta$  are shape and scale parameters, respectively, related to our physiological variables as  $\text{MTT} = \alpha/\beta$  and  $\text{CTH} = \beta\sqrt{\alpha}$ . We further computed the coefficient of variation  $\text{RTH} = \text{CTH}/\text{MTT}$  (30).

Finally, we computed relative blood volume within each image voxel as:

$$\text{CBV} = \frac{\int C(t) dt}{\int C_a(t) dt},$$

and CBF according to the central volume theorem (21) as  $\text{CBF} = \text{CBV}/\text{MTT}$ .

### MR DSC ROI analyses

Anatomical  $T_1$  MRI data were segmented in MATLAB using SPM12 to obtain individual, nonoverlapping masks of WM, GM, hippocampi, ventricles, and CSF. In each subject and each session, CSF voxels and the 5% voxels with the highest CBV values were excluded from the masks before applying them to the perfusion map. For each ROI, their mean and mean absolute deviation (MAD) were used in the statistical analyses. MAD was preferred as it is a robust measure of variability little influenced by outliers.

### MR DSC SPM analyses

For the SPM analyses, all perfusion images were resampled to  $1 \times 1 \times 1 \text{ mm}^3$  and segmented into WM, GM, and CSF maps. Each segmented perfusion image was smoothed with a  $9 \times 9 \times 9 \text{ mm}^3$  Gaussian kernel and divided by its similarly smoothed mask to restore edge mass. The appropriate masks were applied to each segmented image and all brain segments reassembled to a single perfusion image. Finally, all images were warped into MNI space to facilitate spatial comparison across subjects.

## Anatomical MRI analyses

The participants  $T_1$  images were used in the anatomical analyses of cortical volume and thickness. Cortical thickness and volume were calculated in CAT12 with default parameters (93). Cortical thickness ROIs were specified by the Destrieux cortical atlas and left and right ROIs summed. As this atlas is a surface atlas, it does not match with the Neuromorphometrics atlas. WMHs were visually scored and counted by a trained and blinded medical researcher (L.Ø.).

## Statistical analyses of GM/WM and hippocampus ROI's, neuropsychology, blood pressure, and blood tests including nitrate/nitrite level

Participants were divided into a "younger" and an "older" subject group, dichotomized at the mean age of the participants (52 years). Statistical description of group characteristics (Table S1) was performed by two-sample t test or  $\chi^2$  test as appropriate. The statistical analyses were based on linear mixed models. Initially, a full model comprising the following terms was established:  $y \sim \text{age} \times \text{APOE} \times \text{nitrate intake} + \text{age} \times \text{APOE} \times \text{session} + \text{BMI} + \text{Gender} + \text{Group} + \text{Educational years} + (1| \text{Participant})$ , where  $y$  is the response variable. The fixed effects of age group, APOE and nitrate intake, as well as their interactions were our primary interest. The term  $\text{age} \times \text{APOE} \times \text{session}$  was included to model out session effects in the age and APOE groups. BMI (or weight and height separately in the perfusion analysis as CM was administered according to weight, and height is related to brain size (94)), gender, and educational years were included as they were assumed important in modeling effects related to the brain and vasculature. Group was included to model out effects of inequalities in the two groups used to create the cross-over part of the study.

APOE, age group, nitrate intake, gender, group, and session were treated as categorical variables belonging to one of the

following two groups: APOE ( $\epsilon 4$  carrier or control); age group (younger or older); nitrate intake (NaNO<sub>3</sub> or NaCl); session (first or second); group (A or B); and gender (male or female). BMI (kg/m<sup>2</sup>), height (cm), weight (kg), and educational years (years of education) were computed as normalized continuous variables. This full model was iteratively reduced by defining a *P*-threshold of 0.05 and successively removing the model term with the largest supra-threshold *P*-value until all terms remained below the *P*-threshold. Final significance of the remaining model terms was judged based on a second *P*-threshold to account for multiple tests (details provided below).

### Stepwise regression analyses for sub-ROIs

To complement our ROI analysis restricted to WM, GM, and hippocampus, we performed a stepwise regression analysis on smaller sub-ROIs defined by CAT 12 Neuromorphometrics atlas. As we had no hypothesis regarding sidedness, left and right hemisphere ROIs were, when applicable, grouped. This left us with 64 ROIs. Only voxels with between 0.8 and 1.0 tissue probability were used, and the ROI category (GM or WM) had to match across all participants. To be less influenced by potential outliers in these smaller ROIs, we used medians to summarize metrics across them. Also, an outlier removal step was included, and participant ROIs at more than 0.5 Cook's distance were not considered. The initial model for interrogating age and APOE effects was simplified and formulated as:  $y \sim \text{age} \times \text{APOE} + \text{nitrate intake} + \text{LDL} + \text{BMI} + \text{Gender} + \text{Educational years}$ , where *y* is the response variable, age is the age in years, APOE grouped in carrier or control, nitrate intake is NO<sub>3</sub> or NaCl intake, LDL is the low-density lipoprotein in mmol/l, BMI = kg/m<sup>2</sup>, gender as male or female, and educational years as years of education. APOE, gender, and nitrate intake were computed as categorical variables and the rest as normalized continuous variables. The decision to include LDL was taken retrospectively as it was seen to improve our models. The criterion for model reduction was change in the value of the Akaike information criterion. As a final check, only reduced models statistically different (<0.05) from a null/intercept model were retained for comparison. To be able to compare the final reduced model from the stepwise reduction with the LME models from the initial analysis, the final reduced models was also calculated in an LME version with participants included as random factors. To analyze cortical thickness, the same stepwise regression pipeline was used.

### Thresholds for statistical significance

We applied Bonferroni's correction to account for multiple tests:

#### Blood samples—nitrate/nitrite

The *P*-threshold was set to  $0.05/2 = 0.025$  as both nitrite and nitrate were tested.

#### Neuropsychological tests

The *P*-threshold was set to  $0.05/6 = 0.0083$  as six independent tests were conducted.

#### Blood pressure

The *P*-threshold was set to  $0.05/2 = 0.025$  as both diastolic and systolic blood pressure was tested.

### MR DSC ROI analysis

As two main parameters ( $\alpha$  and  $\beta$ ) are the basis for all the perfusion maps computed across three tissue types (WM, GM, and hippocampi), a threshold of  $0.05/6 = 0.0083$  was considered as the *P*-threshold for significance.

### MR DSC SPM analyses

Voxel-wise factorial analyses were carried out in SPM12. The design matrix was based on eight main groups created based on APOE status, nitrate intake, and age group. Nitrate ingestion was considered as a dependent factor with equal variance across levels, whereas APOE status and age group were considered as independent factors with unequal variance across levels. Weight, gender, APOE allele status, age, plasma nitrate, and transcutaneous PCO<sub>2</sub> and SpO<sub>2</sub> were included as group mean-centered regressors. No other intensity normalization or scaling procedures were carried out on the data. To be considered significant, the SPM maps had to contain clusters with a family-wise error (FWE) adjusted *P*-value  $\leq 0.01$ , in maps with an uncorrected voxel-wise threshold  $\leq 0.001$ .

### Stepwise regression analyses for sub-ROIs

These analyses were used to support the initial analyses and to investigate the factors impacting several sub-ROIs. Therefore, no specific threshold for statistical significance was specified, but the standard limits of  $P < 0.05$  and  $P < 0.01$  were used to filter the results and clarify their patterns.

## Supplementary Material

Supplementary material is available at PNAS Nexus online.

## Funding

This study was supported by the VELUX Foundation (Healthy Ageing with Nitrate, grant no. 19784, R.A. and P.M.R.), the Lundbeck Foundation (Professorship grant no. R310-2018-3455, R.A. and L.Ø.), and the Danish Ministry of Science, Technology and Innovation's UNIK program (MINDLab, T.E.L.).

## Author Contributions

R.A., T.E.L., and L.Ø. conceived the study. R.A., S.P., T.E.L., and L.Ø. developed the study design. R.A., K.S.A., and T.E.L. acquired the data. E.W. determined plasma nitrate and nitrite content. M.C. determined APOE genotype. R.A. drafted the manuscript, and L.Ø. made substantive revisions. All authors contributed to the analysis, interpreted the data, revised the manuscript, and approved the submitted version.

## Data Availability

The authors are happy to share all data upon request and written agreement.

## References

- 1 Corder EH, et al. 1993. Gene dose of apolipoprotein E type 4 allele and the risk of Alzheimer's disease in late onset families. *Science*. 261:921–923.
- 2 Scarmeas N, Habeck CG, Stern Y, Anderson KE. 2003. APOE genotype and cerebral blood flow in healthy young individuals. *JAMA*. 290:1581–1582.



- 3 Bracko O, Cruz Hernández JC, Park L, Nishimura N, Schaffer CB. 2021. Causes and consequences of baseline cerebral blood flow reductions in Alzheimer's disease. *J Cereb Blood Flow Metab.* 41:1501–1516.
- 4 Hays CC, Zlatar ZZ, Wierenga CE. 2016. The utility of cerebral blood flow as a biomarker of preclinical Alzheimer's disease. *Cell Mol Neurobiol.* 36:167–179.
- 5 Wierenga CE, et al. 2013. Interaction of age and APOE genotype on cerebral blood flow at rest. *J Alzheimers Dis.* 34:921–935.
- 6 Fleisher AS, et al. 2009. Cerebral perfusion and oxygenation differences in Alzheimer's disease risk. *Neurobiol Aging.* 30:1737–1748.
- 7 Thambisetty M, Beason-Held L, An Y, Kraut MA, Resnick SM. 2010. APOE epsilon4 genotype and longitudinal changes in cerebral blood flow in normal aging. *Arch Neurol.* 67:93–98.
- 8 McKiernan EF, et al. 2020. Regional hyperperfusion in cognitively normal APOE epsilon4 allele carriers in mid-life: analysis of ASL pilot data from the PREVENT-dementia cohort. *J Neurol Neurosurg Psychiatry.* 91:861–866.
- 9 Dounavi ME, et al. 2021. Evidence of cerebral hemodynamic dysregulation in middle-aged APOE epsilon4 carriers: the PREVENT-dementia study. *J Cereb Blood Flow Metab.* 41:2844–2855.
- 10 Bookheimer SY, et al. 2000. Patterns of brain activation in people at risk for Alzheimer's disease. *N Engl J Med.* 343:450–456.
- 11 Scarmeas N, et al. 2005. APOE related alterations in cerebral activation even at college age. *J Neurol Neurosurg Psychiatry.* 76:1440–1444.
- 12 Filippini N, et al. 2011. Differential effects of the APOE genotype on brain function across the lifespan. *Neuroimage.* 54:602–610.
- 13 Zlatar ZZ, et al. 2016. Higher brain perfusion may not support memory functions in cognitively normal carriers of the ApoE epsilon 4 allele compared to non-carriers. *Front Aging Neurosci.* 8:151.
- 14 Filippini N, et al. 2009. Distinct patterns of brain activity in young carriers of the APOE-epsilon4 allele. *Proc Natl Acad Sci U S A.* 106:7209–7214.
- 15 Ringman JM, et al. 2011. Effects of risk genes on BOLD activation in presymptomatic carriers of familial Alzheimer's disease mutations during a novelty encoding task. *Cerebral Cortex.* 21:877–883.
- 16 Trachtenberg AJ, et al. 2012. The effects of APOE on brain activity do not simply reflect the risk of Alzheimer's disease. *Neurobiol Aging.* 33:618.e1–618.e13.
- 17 Tai LM, et al. 2016. The role of APOE in cerebrovascular dysfunction. *Acta Neuropathol.* 131:709–723.
- 18 Zlokovic BV. 2013. Cerebrovascular effects of apolipoprotein E: implications for Alzheimer disease. *JAMA Neurol.* 70:440–444.
- 19 Østergaard L, et al. 2013. The capillary dysfunction hypothesis of Alzheimer's disease. *Neurobiol Aging.* 34:1018–1031.
- 20 Østergaard L. 2020. Blood flow, capillary transit times, and tissue oxygenation. The centennial of capillary recruitment. *J Appl Physiol (1985).* 129:1413–1421.
- 21 Stewart GN. 1893. Researches on the circulation time in organs and on the influences which affect it. Parts I.-III. *J Physiol.* 15:1–89.
- 22 Klein B, Kuschinsky W, Schrock H, Vetterlein F. 1986. Interdependency of local capillary density, blood flow, and metabolism in rat brains. *Am J Physiol.* 251:H1333–H1340.
- 23 Kuschinsky W, Paulson OB. 1992. Capillary circulation in the brain. *Cerebrovasc Brain Metab Rev.* 4:261–286.
- 24 Kleinfeld D, Mitra PP, Helmchen F, Denk W. 1998. Fluctuations and stimulus-induced changes in blood flow observed in individual capillaries in layers 2 through 4 of rat neocortex. *Proc Natl Acad Sci U S A.* 95:15741–15746.
- 25 Villringer A, Them A, Lindauer U, Einhaupl K, Dirnagl U. 1994. Capillary perfusion of the rat brain cortex. An in vivo confocal microscopy study. *Circ Res.* 75:55–62.
- 26 Stefanovic B, et al. 2008. Functional reactivity of cerebral capillaries. *J Cereb Blood Flow Metab.* 28:961–972.
- 27 Rasmussen PM, Jespersen SN, Østergaard L. 2015. The effects of transit time heterogeneity on brain oxygenation during rest and functional activation. *J Cereb Blood Flow Metab.* 35:432–442.
- 28 Jespersen SN, Østergaard L. 2012. The roles of cerebral blood flow, capillary transit time heterogeneity and oxygen tension in brain oxygenation and metabolism. *J Cereb Blood Flow Metab.* 32:264–277.
- 29 Angleys H, Østergaard L, Jespersen SN. 2015. The effects of capillary transit time heterogeneity (CTH) on brain oxygenation. *J Cereb Blood Flow Metab.* 35:806–817.
- 30 Mouridsen K, Hansen MB, Østergaard L, Jespersen SN. 2014. Reliable estimation of capillary transit time distributions using DSC-MRI. *J Cereb Blood Flow Metab.* 34:1511–1521.
- 31 Boxerman JL, Hamberg LM, Rosen BR, Weisskoff RM. 1995. MR contrast due to intravascular magnetic susceptibility perturbations. *Magn Reson Med.* 34:555–566.
- 32 Goense JBM, Logothetis NK. 2006. Laminar specificity in monkey V1 using high-resolution SE-fMRI. *Magn Reson Imaging.* 24:381–392.
- 33 Eskildsen SF, et al. 2017. Increased cortical capillary transit time heterogeneity in Alzheimer's disease: a DSC-MRI perfusion study. *Neurobiol Aging.* 50:107–118.
- 34 Nielsen RB, et al. 2020. Impaired perfusion and capillary dysfunction in prodromal Alzheimer's disease. *Alzheimers Dement (Amst).* 12:e12032.
- 35 Madsen LS, et al. 2023. Capillary dysfunction correlates with cortical amyloid load in early Alzheimer's disease. *Neurobiol Aging.* 123:1–9.
- 36 Madsen LS, et al. 2024. Capillary dysfunction in healthy elderly APOE ε4 carriers with raised brain aβ deposition. *Alzheimers Dement.* 20(1):459–471.
- 37 Madsen LS, et al. 2022. Capillary function progressively deteriorates in prodromal Alzheimer's disease: a longitudinal MRI perfusion study. *Aging Brain.* 2:100035.
- 38 Nielsen RB, et al. 2017. Capillary dysfunction is associated with symptom severity and neurodegeneration in Alzheimer's disease. *Alzheimer's & dementia.* 13:1143–1153.
- 39 Jack CR Jr, et al. 2013. Tracking pathophysiological processes in Alzheimer's disease: an updated hypothetical model of dynamic biomarkers. *Lancet Neurol.* 12:207–216.
- 40 Nortley R, et al. 2019. Amyloid beta oligomers constrict human capillaries in Alzheimer's disease via signaling to pericytes. *Science.* 365(6450):eaav9518.
- 41 Goirand F, Borgne TL, Lorthois S. 2021. Network-driven anomalous transport is a fundamental component of brain microvascular dysfunction. *Nat Commun.* 12:7295.
- 42 Sun X, et al. 2006. Hypoxia facilitates Alzheimer's disease pathogenesis by up-regulating BACE1 gene expression. *Proc Natl Acad Sci U S A.* 103:18727–18732.
- 43 Jansen WJ, et al. 2015. Prevalence of cerebral amyloid pathology in persons without dementia: a meta-analysis. *JAMA.* 313:1924–1938.
- 44 Jack CR Jr, et al. 2014. Age-specific population frequencies of cerebral beta-amyloidosis and neurodegeneration among people with normal cognitive function aged 50–89 years: a cross-sectional study. *Lancet Neurol.* 13:997–1005.



- 45 Wardlaw JM, et al. 2013. Neuroimaging standards for research into small vessel disease and its contribution to ageing and neurodegeneration. *Lancet Neurol.* 12:822–838.
- 46 Dalby RB, et al. 2019. Oxygenation differs among white matter hyperintensities, intersected fiber tracts and unaffected white matter. *Brain Commun.* 1:fcz033.
- 47 Schilling S, et al. 2013. APOE genotype and MRI markers of cerebrovascular disease: systematic review and meta-analysis. *Neurology.* 81:292–300.
- 48 Rojas S, et al. 2018. Higher prevalence of cerebral white matter hyperintensities in homozygous APOE-varepsilon4 allele carriers aged 45–75: results from the ALFA study. *J Cereb Blood Flow Metab.* 38:250–261.
- 49 Fazekas F, Chawluk JB, Alavi A, Hurtig HI, Zimmerman RA. 1987. MR signal abnormalities at 1.5 T in Alzheimer's dementia and normal aging. *AJR Am J Roentgenol.* 149:351–356.
- 50 Stern Y, et al. 1994. Influence of education and occupation on the incidence of alzheimers-disease. *JAMA.* 271:1004–1010.
- 51 Xu W, et al. 2016. Education and risk of dementia: dose-response meta-analysis of prospective cohort studies. *Mol Neurobiol.* 53:3113–3123.
- 52 Attwell D, et al. 2010. Glial and neuronal control of brain blood flow. *Nature.* 468:232–243.
- 53 Iadecola C, Gottesman RF. 2019. Neurovascular and cognitive dysfunction in hypertension. *Circ Res.* 124:1025–1044.
- 54 Park L, et al. 2017. Brain perivascular macrophages initiate the neurovascular dysfunction of Alzheimer abeta peptides. *Circ Res.* 121:258–269.
- 55 Koizumi K, et al. 2018. Apo epsilon 4 disrupts neurovascular regulation and undermines white matter integrity and cognitive function. *Nat Commun.* 9:3816.
- 56 Sacre SM, Stannard AK, Owen JS. 2003. Apolipoprotein E (apoE) isoforms differentially induce nitric oxide production in endothelial cells. *FEBS Lett.* 540:181–187.
- 57 Duncan C, et al. 1995. Chemical generation of nitric oxide in the mouth from the enterosalivary circulation of dietary nitrate. *Nat Med.* 1:546–551.
- 58 Lundberg JO, Weitzberg E. 2005. NO generation from nitrite and its role in vascular control. *Arterioscler Thromb Vasc Biol.* 25:915–922.
- 59 Clifford T, et al. 2019. Effects of inorganic nitrate and nitrite consumption on cognitive function and cerebral blood flow: a systematic review and meta-analysis of randomized clinical trials. *Crit Rev Food Sci Nutr.* 59:2400–2410.
- 60 Larsen FJ, et al. 2011. Dietary inorganic nitrate improves mitochondrial efficiency in humans. *Cell Metab.* 13:149–159.
- 61 Ashworth A, Bescos R. 2017. Dietary nitrate and blood pressure: evolution of a new nutrient? *Nutr Res Rev.* 30:208–219.
- 62 Shin MS, Park SY, Park SR, Seol SH, Kwon JS. 2006. Clinical and empirical applications of the Rey-Osterrieth complex figure test. *Nat Protoc.* 1:892–899.
- 63 Tombaugh TN. 2004. Trail making test A and B: normative data stratified by age and education. *Arch Clin Neuropsych.* 19:203–214.
- 64 Alata W, Ye Y, St-Amour I, Vandal M, Calon F. 2015. Human apolipoprotein E varepsilon4 expression impairs cerebral vascularization and blood-brain barrier function in mice. *J Cereb Blood Flow Metab.* 35:86–94.
- 65 Bell RD, et al. 2012. Apolipoprotein E controls cerebrovascular integrity via cyclophilin A. *Nature.* 485:512–516.
- 66 Shaw K, et al. 2021. Neurovascular coupling and oxygenation are decreased in hippocampus compared to neocortex because of microvascular differences. *Nat Commun.* 12:3190.
- 67 Zatorre RJ, Fields RD, Johansen-Berg H. 2012. Plasticity in gray and white: neuroimaging changes in brain structure during learning. *Nat Neurosci.* 15:528–536.
- 68 Sampaio-Baptista C, Johansen-Berg H. 2017. White matter plasticity in the adult brain. *Neuron.* 96:1239–1251.
- 69 Harris JJ, Jolivet R, Attwell D. 2012. Synaptic energy use and supply. *Neuron.* 75:762–777.
- 70 Li B, et al. 2019. More homogeneous capillary flow and oxygenation in deeper cortical layers correlate with increased oxygen extraction. *Elife.* 8:e42299.
- 71 Østergaard L, et al. 2015. Capillary dysfunction: its detection and causative role in dementias and stroke. *Curr Neurol Neurosci Rep.* 15:37.
- 72 Smith AF, et al. 2019. Brain capillary networks across Species: a few simple organizational requirements are sufficient to reproduce both structure and function. *Front Physiol.* 10:233.
- 73 Bassingthwaite JB, King RB, Roger SA. 1989. Fractal nature of regional myocardial blood flow heterogeneity. *Circ Res.* 65:578–590.
- 74 Gutierrez-Jimenez E, et al. 2018. Disturbances in the control of capillary flow in an aged APP(swe)/PS1DeltaE9 model of Alzheimer's disease. *Neurobiol Aging.* 62:82–94.
- 75 Wightman EL, et al. 2015. Dietary nitrate modulates cerebral blood flow parameters and cognitive performance in humans: a double-blind, placebo-controlled, crossover investigation. *Physiol Behav.* 149:149–158.
- 76 Aamand R, et al. 2013. A NO way to BOLD? : dietary nitrate alters the hemodynamic response to visual stimulation. *Neuroimage.* 83C:397–407.
- 77 Alexander A, et al. 2008. Nitrate in vegetables. Scientific opinion of the panel on contaminants in the food chain. *EFSA J.* 689:1–79.
- 78 Rasmussen PM, et al. 2019. APOE gene-dependent BOLD responses to a breath-hold across the adult lifespan. *Neuroimage Clin.* 24:101955.
- 79 Langbaum JB, et al. 2014. An empirically derived composite cognitive test score with improved power to track and evaluate treatments for preclinical Alzheimer's disease. *Alzheimers Dement.* 10:666–674.
- 80 Joubert S, et al. 2016. Early-onset and late-onset Alzheimer's disease are associated with distinct patterns of memory impairment. *Cortex.* 74:217–232.
- 81 Wechsler D. 2008. *WAIS-IV Technical and interpretive manual* 4th ed. Pearson/PsychCorp, San Antonio, Texas, vol. 1, pp. 218.
- 82 Wechsler D, 1997, *Wechsler adult intelligence scale.* 3<sup>rd</sup> ed. The Psychological Corporation, San Antonio, Texas, vol. 1.
- 83 Ruff R, Light R, Parker S. 1996. Visuospatial learning: ruff light trail learning test. *Arch Clin Neuropsych.* 11:313–327.
- 84 Raven JC, Court JH. 2004. *Manual for Raven's Progressive matrices and vocabulary scales.* Oxford Psychologists Press, Oxford.
- 85 Weisskoff RM, Zuo CS, Boxerman JL, Rosen BR. 1994. Microscopic susceptibility variation and transverse relaxation: theory and experiment. *Magn Reson Med.* 31:601–610.
- 86 Nael K, et al. 2014. Six-minute magnetic resonance imaging protocol for evaluation of acute ischemic stroke: pushing the boundaries. *Stroke.* 45:1985–1991.
- 87 Andersson JLR, Skare S, Ashburner J. 2003. How to correct susceptibility distortions in spin-echo echo-planar images: application to diffusion tensor imaging. *Neuroimage.* 20:870–888.
- 88 Østergaard L, Weisskoff RM, Chesler DA, Gyldensted C, Rosen BR. 1996. High resolution measurement of cerebral blood flow using intravascular tracer bolus passages. Part I: mathematical approach and statistical analysis. *Magn Reson Med.* 36:715–725.

- 
- 89 Kjolby B, Mikkelsen I, Pedersen M, Østergaard L, Kiselev V. 2009. Analysis of partial volume effects on arterial input functions using gradient Echo: a simulation study. *Magn Reson Med.* 61: 1300–1309.
- 90 van Osch MJ, van der Grond J, Bakker CJ. 2005. Partial volume effects on arterial input functions: shape and amplitude distortions and their correction. *J Magn Reson Imaging.* 22:704–709.
- 91 Mouridsen K, Christensen S, Gyldensted L, Østergaard L. 2006. Automatic selection of arterial input function using cluster analysis. *Magn Reson Med.* 55:524–531.
- 92 Mouridsen K, et al. 2006. Bayesian estimation of cerebral perfusion using a physiological model of microvasculature. *NeuroImage.* 33:570–579.
- 93 Christian G, et al., CAT—A Computational Anatomy Toolbox for the Analysis of Structural MRI Data. bioRxiv 495736. <https://doi.org/10.1101/2022.06.11.495736>, 13 June 2022, preprint: not peer reviewed.
- 94 Dekaban AS. 1978. Changes in brain weights during the span of human life: relation of brain weights to body heights and body weights. *Ann Neurol.* 4:345–356.